Journal of Organometallic Chemistry, 423 (1992) 241–254
Elsevier Sequoia S.A., Lausanne
JOM 22235

$Ru_3(CO)_9BH_5$ and $[Ru_3(CO)_9BH_4]^-$ as precursors to higher nuclearity homo- and heterometallic clusters: molecular structure of a second isomer of $HRu_6(CO)_{17}B$

Sylvia M. Draper, Catherine E. Housecroft*, Ann K. Keep, Dorn M. Matthews, Xuejing Song

University Chemical Laboratory, Lensfield Road, Cambridge CB2 1EW (UK)

and Arnold L. Rheingold*

Department of Chemistry, University of Delaware, Newark DE 19716 (USA)

(Received July 3, 1991)

Abstract

The cluster $Ru_3(CO)_9BH_5$, which contains four bridging (Ru–H–Ru or Ru–H–B) hydrogen atoms, spontaneously forms $HRu_4(CO)_{12}BH_2$ and $HRu_6(CO)_{17}B$ on standing in solution at room temperature. The transformations are also observed upon photolysis of $Ru_3(CO)_9BH_5$. A crystallographic study of $HRu_6(CO)_{17}B$ has revealed a new structural isomer in which the boron atom resides at the centre of a distorted octahedral Ru_6-cavity. $Ru_3(CO)_9BH_5$ reacts with $Fe(CO)_5$ under photolytic conditions to give $HRu_3Fe(CO)_{12}BH_2$, in which the iron atom appears to reside exclusively at a wingtip site. This heterometallic cluster deprotonates by loss of the Fe–H–B proton to give $[HRu_3Fe(CO)_{12}BH]^-$ and this anion may also be generated by the direct reaction of $[Ru_3(CO)_9BH_4]^-$ with $Fe(CO)_5$. Both $HRu_3Fe(CO)_{12}BH_2$ and $[HRu_3Fe(CO)_{12}BH]^-$ are static on the NMR timescale at room temperature. The solution properties of $[Ru_3(CO)_9BH_4]^-$ are reported, and are compared with those of the conjugate acid.

Introduction

We have previously reported the synthesis and spectroscopic characterisation of the triruthenium cluster $Ru_3(CO)_9BH_5$ (**1**) [1]. One interesting feature of this metalloborane is that in solution it exists in two isomeric forms, **1a** and **1b**, that are equally populated at room temperature. At temperatures $\geqslant 373$ K the isomers interconvert on the 250 MHz timescale [1]. It was of interest to us to study the reactivity of **1** and in particular to investigate whether there was any difference in the relative reactivities of **1a** and **1b**. The potential reactivity of **1** became apparent when we noted that, on standing in solution at room temperature or even at $-10\,^{\circ}C$, **1** spontaneously converted to a mixture of $HRu_4(CO)_{12}BH_2$ (**2**) [2–4] and $HRu_6(CO)_{17}B$ (**3**) [5]. Compounds **2** and **3** are easily distinguished from **1** by their characteristic downfield resonances in the ^{11}B NMR spectrum [3–5]. Cluster expansion reactions from a cluster of core type M_3E to one of type M_4E or $M_3M'E$ (M and M′ = transition metal, E = *p*-block element) have been docu-

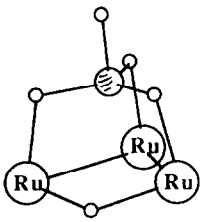

1 a

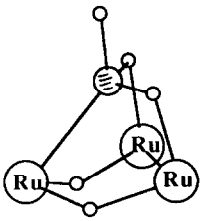

1 b

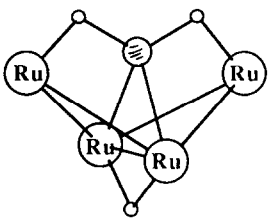

2

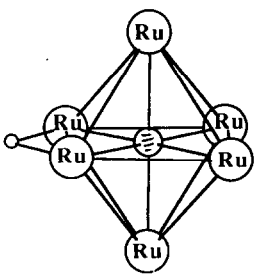

3

mented for E = B [6,7], C [8–10] and O [11]. For boron, reaction of the anion $[HFe_3(CO)_9BH_3]^-$ with $Fe_2(CO)_9$ leads to $[HFe_4(CO)_{12}BH]^-$ [6,7]. For carbon, carbide clusters such as $[Fe_3Rh(CO)_{12}C]^-$, $[Fe_3Mn(CO)_{13}C]^-$, $[Fe_3Cr(CO)_{13}C]^{2-}$ and $[Fe_3W(CO)_{13}C]^{2-}$ have been prepared via reaction of the ketenylidene cluster $[Fe_3(CO)_9CCO]^{2-}$ with $[Rh(CO)_2Cl]_2$, $[Mn(CO)_5(NCMe)]^+$, $Cr(CO)_3(NCMe)_3$ and $W(CO)_3(NCMe)_3$ respectively [8–10]. In the case of oxygen, the oxo-cluster $[Fe_3Mn(CO)_{12}O]^-$ is formed when $[Fe_3(CO)_9O]^{2-}$ is combined with $[Mn(CO)_5(NCMe)]^+$ [11]. The synthesis of heterometallic clusters is of particular interest since the introduction of the heterometal should perturb the electronic structure of the metal cage quite significantly [10]. In some cases, reaction pathways which compete with the straight addition of one metal fragment have been reported. For example, the substitution of cobalt for iron during the reaction of $[Fe_3(CO)_9CCO]^{2-}$ with $Co_2(CO)_8$ [8], or the continued reaction to higher nuclearity clusters such as $[Fe_3Ni_3(CO)_{13}C]^-$ or $[Fe_4Co(CO)_{14}C]^-$ [9].

In this paper we report an investigation of the spontaneous cluster expansion of **1** to form the butterfly cluster **2** and the *closo*-boride cluster **3** and we explore the introduction of an iron tricarbonyl fragment to generate $HRu_3Fe(CO)_{12}BH_2$.

Experimental

General data

Synthetic steps were carried out under argon. Solvents were dried and distilled prior to use. Thin layer chromatography was carried out on Kieselgel 60-F_{254}

(Merck) in tanks flushed with nitrogen. PPNCl (PPN = bis(triphenylphosphine)nitrogen(1 +)) and $Fe(CO)_5$ were used as received (Aldrich). $Ru_3(CO)_9BH_5$ (**1**) was prepared as previously reported [1]. FT-NMR spectra were recorded on a Bruker AM 400 or 250 spectrometer. ^1H NMR chemical shifts are reported with respect to $\delta = 0$ ppm for Me_4Si and ^{11}B NMR with respect $\delta = 0$ ppm for $F_3B \cdot OEt_2$. All downfield chemical shifts are positive. Infrared spectra were recorded on a Perkin–Elmer FT 1710 spectrophotometer. Mass spectra were recorded on a Kratos MS 890 instrument. Photolysis experiments used a mercury high-pressure lamp (Aldrich).

Photolysis of $Ru_3(CO)_9BH_5$ (1)

1 (0.04 g, 0.07 mmol) was dissolved in CD_2Cl_2 (0.5 ml) in a quartz tube and the resulting deep yellow solution was photolysed for 16 h. ^{11}B NMR spectroscopic data for the crude reaction mixture showed the presence of **2** [2–4] and **3** [5] in addition to unreacted **1**. The products were separated by TLC eluting with hexane: the first (yellow) band was unreacted **1**, the second (deep yellow) band was $H_4Ru_4(CO)_{12}$ ($\approx 10\%$), the third (yellow) fraction was **2** ($\approx 50\%$) and the final (brown) band which remained close to the baseline was **3** ($\approx 10\%$). The IR, mass and ^1H and ^{11}B NMR spectroscopic data for each compound were consistent with the published data (see text for **3**) [2–5].

Photolysis of 1 with $Fe(CO)_5$

1 (0.07 g, 0.12 mmol) was placed in a quartz tube with $Fe(CO)_5$ (0.25 ml, 1.79 mmol) and CD_2Cl_2 (0.5 ml). The solution was photolysed and was monitored at intervals by use of ^{11}B NMR spectroscopy. **1** had been completely consumed in 95 min with the formation of a single cluster product identified as $HRu_3Fe(CO)_{12}BH_2$. The product was separated by TLC (hexane eluent) as the third (yellow) band in $\approx 60\%$ yield; the fourth (dark green) fraction was identified as $Fe_3(CO)_{12}$. Five other bands were observed, each in insufficient quantity to analyse. $HRu_3Fe(CO)_{12}BH_2$: 128 MHz ^{11}B NMR ($CDCl_3$, 298 K) $\delta + 114$ (apparent triplet, $J(BH) \approx 65$ Hz); 250 MHz ^1H NMR ($CDCl_3$, 298 K) $\delta - 8.7$ (br. quartet, $J(BH) \approx 60$ Hz, Ru–H–B), -11.2 (br. quartet, $J(BH) \approx 60$ Hz, Fe–H–B), -20.5 (s, Ru–H–Ru); IR (hexane, cm^{-1}) ν(CO) 2067vs, 2043m, 2024m, 1995sh; EI-MS P^+ 711 (calcd. and obsd. isotopic distributions in agreement $C_{12}H_3BFeO_{12}Ru_3$).

Preparation of [PPN][$Ru_3(CO)_9BH_4$]

In a typical reaction a solution of **1** (0.05 g, 0.09 mmol) in acetone (5 ml) was added to a methanol solution (5 ml) containing [PPN]Cl (0.05 g, 0.09 mmol) and Na_2CO_3 (5.30 mg, 0.05 mmol). The mixture was stirred for 15 min after which time solvent was removed. The solid residue was washed with hexane to remove unreacted **1** and then the anionic product was extracted with Et_2O (2×10 ml). [PPN][$Ru_3(CO)_9BH_4$]: 128 MHz ^{11}B NMR ($(CD_3)_2CO$, 298 K) $\delta + 22.5$; 250 MHz ^1H NMR ($(CD_3)_2CO$, 298 K) $\delta + 7.9$–7.5 (m, PPN) + 3.5 (br, 1H), -12.1 (br, 3H); IR (CH_2Cl_2, cm^{-1}) ν(CO) 2035s, 2020vs, 2002s, 1995sh, 1971m, 1950sh; FAB-MS (NBA matrix) P^- 572 (calcd. and obsd. isotopic distributions in agreement for $C_9H_4BO_9Ru_3$).

Reaction of [PPN][$Ru_3(CO)_9BH_4$] with $Fe(CO)_5$

[PPN][$Ru_3(CO)_9BH_4$] (0.11 g, 0.10 mmol) was combined with $Fe(CO)_5$ (0.14 ml, 1.00 mmol) and THF (2 ml) was added. The solution was stirred for 40 min and then solvent and excess $Fe(CO)_5$ were removed. Hexane (10 ml) followed by CF_3CO_2H (0.25 ml) were added to the crude solid. After 25 min of constant stirring, the hexane layer had turned green-yellow in colour. The mixture was filtered and the filtrate collected and reduced to dryness. The products were separated by TLC, eluting with hexane. The third (yellow) band was the major fraction and was identified as $HRu_3Fe(CO)_{12}BH_2$ (yield < 10%).

Formation of [PPN][$HRu_3Fe(CO)_{12}BH$]

[PPN][$HRu_3Fe(CO)_{12}BH$] may be prepared by the first part of the route described above but separation of the neutral rather than the anionic metalloborane is more easily achieved. Thus, ether soluble red-orange [PPN][$HRu_3Fe(CO)_{12}BH$] is more conveniently prepared by deprotonating $HRu_3Fe(CO)_{12}BH_2$ in a solution of MeOH containing Na_2CO_3 and [PPN]Cl. A typical procedure is as for [PPN][$Ru_3(CO)_9BH_4$]. [PPN][$HRu_3Fe(CO)_{12}BH$]: 128 MHz ^{11}B NMR (CD_2Cl_2, 298 K) δ + 139.4 (d, J(BH) 90 Hz); 250 MHz ^1H NMR (CD_2Cl_2, 298 K) δ + 7.8–7.5 (m, PPN), −6.5 (br, Ru–H–B), −20.5 (s, Ru–H–Ru); IR (CH_2Cl_2, cm^{-1}) ν(CO) 2013sh, 1992m, 1953vs, br., 1905sh; FAB-MS (NBA matrix) P^- 708 (calcd. and obsd. isotopic distributions in agreement for $C_{12}H_2BFeO_{12}Ru_3$).

Crystallographic structure determination for ***3a***

Crystallographic data are presented in Table 1 and atomic coordinates in Table 2. A specimen obtained by recrystallisation from CH_2Cl_2 layered with hexane was

Table 1

Crystallographic data for **3a**

Crystal parameters			
Formula	$C_{17}HBO_{17}Ru_6$	Z	4
Formula weight	1094.38	Crystal dimens. (mm)	0.37×0.40×0.44
Crystal system	orthorhombic	Crystal colour	deep red
Space group	$P2_12_12_1$	D_{calc} (g cm^{-3})	2.754
a (Å)	11.954(3)	μ(Mo-K_α) (cm^{-1})	33.6
b (Å)	13.365(3)	Temperature (K)	297
c (Å)	16.520(4)	T(max)/T(min)	0.101/0.072
V (Å^3)	2639.2(13)		
Data collection			
Diffractometer	Nicolet R3m	Reflections collected	7632
Monochromator	graphite	Independent reflections	7597
Radiation	Mo-K_α (λ 0.71073 Å)	Independent reflections	6833 $F_o \geq 4\sigma(F_o)$
2θ scan range (°)	4–58	Std. reflections	3std/197 rflns.
Data collected (h, k, l)	+17, +19, ±23	Var. in standards	< 1
Refinement			
$R(F)$ (%)	3.09	$\Delta(\rho)$ (e Å^{-3})	1.16
$R(wF)$ (%)	3.71	N_o/N_v	18.0
Δ/σ(max)	0.05	GOF	0.878

Table 2

Atomic coordinates ($\times 10^4$) and isotropic thermal parameters ($Å^2 \times 10^3$) for **3a**

Atom	x	y	z	U [a]
Ru(1)	9319.9(4)	406.6(3)	1197.2(2)	32.4(1)
Ru(2)	7807.7(4)	−62.7(3)	−160.6(3)	31.3(1)
Ru(3)	9831.8(4)	−631.4(4)	−1133.2(3)	35.4(1)
Ru(4)	11259.9(4)	246.4(3)	94.5(3)	32.4(1)
Ru(5)	9452.0(4)	1429.0(3)	−449.4(3)	36.0(1)
Ru(6)	9529.1(4)	−1526.7(3)	441.5(3)	33.7(1)
B	9528(5)	−53(4)	6(3)	30(1)
O(1)	7521(5)	−431(5)	2307(3)	69(2)
O(2)	11067(6)	−113(6)	2466(3)	85(3)
O(3)	8977(6)	2518(4)	1878(4)	76(2)
O(4)	5920(5)	433(5)	1019(3)	75(2)
O(5)	6071(4)	−866(4)	−1338(3)	59(2)
O(6)	6967(4)	1832(4)	−973(3)	59(2)
O(7)	8217(5)	−1792(5)	−2181(3)	69(2)
O(8)	10682(8)	530(7)	−2591(3)	111(4)
O(9)	11577(5)	−2254(6)	−1335(4)	85(2)
O(10)	13263(5)	−461(5)	−878(4)	71(2)
O(11)	11860(4)	2204(4)	−693(3)	59(2)
O(12)	12862(6)	961(6)	1414(4)	83(3)
O(13)	9361(5)	3511(4)	257(4)	66(2)
O(14)	9492(6)	2448(5)	−2079(3)	86(3)
O(15)	8858(6)	−2477(4)	2063(3)	72(2)
O(16)	9365(6)	−3457(4)	−548(4)	73(2)
O(17)	11924(4)	−2041(5)	909(4)	83(3)
C(1)	8168(6)	−112(5)	1876(4)	47(2)
C(2)	10422(7)	97(6)	1980(4)	54(2)
C(3)	9086(6)	1758(5)	1599(4)	46(2)
C(4)	6633(6)	237(5)	579(4)	49(2)
C(5)	6758(6)	−611(5)	−918(4)	46(2)
C(6)	7579(5)	1298(5)	−671(4)	41(2)
C(7)	8766(5)	−1345(5)	−1787(4)	47(2)
C(8)	10321(8)	113(7)	−2036(4)	69(3)
C(9)	10945(6)	−1639(7)	−1283(4)	55(2)
C(10)	12503(5)	−205(5)	−533(4)	47(2)
C(11)	11265(5)	1578(5)	−447(4)	47(2)
C(12)	12272(6)	688(6)	920(4)	51(2)
C(13)	9360(5)	2713(4)	2(4)	42(2)
C(14)	9467(6)	2061(6)	−1471(4)	52(2)
C(15)	9094(6)	−2133(5)	1466(4)	43(2)
C(16)	9391(6)	−2732(5)	−176(4)	53(2)
C(17)	11098(6)	−1767(6)	708(4)	53(2)

[a] Equivalent isotropic U defined as one third of the trace of the orthogonalized U_{ij} tensor.

mounted on a fine glass fibre. Photographic evidence revealed *mmm* Laue symmetry; systematic absences in the data uniquely defined the space group. An empirical correction for absorption was applied to the data. The metal atoms were located by direct methods and the structure was completed from subsequent difference Fourier syntheses. All non-hydrogen atoms were refined with anisotropic thermal parameters. The hydrogen atom was neither located nor calculated. All calculations used SHELXTL software (5.1) (G.M. Sheldrick, Nicolet, Madison, WI).

Results and discussion

Formation of $HRu_4(CO)_{12}BH_2$ and $HRu_6(CO)_{17}B$ from $Ru_3(CO)_9BH_5$

When a solution of **1** in dichloromethane was left to stand at room temperature, the composition of the solution gradually changed with **2** and **3** growing in along with some $H_4Ru_4(CO)_{12}$. After one month, approximately 20% of the original starting material remained and, based on ^{11}B NMR spectral data, the yields of **2** and **3** were approximately 40 and 30%, respectively. These observations indicated the potentially high reactivity of **1**, presumably driven by the ability of the cluster to lose H_2. ^{11}B NMR spectral monitoring of the solution showed that the resonances assigned to isomers **1a** and **1b** disappeared at the same rate as one another. This suggests that **1a** and **1b** are equally reactive with respect to spontaneous cluster growth. However, since **1a** and **1b** are in equilibrium [1], we cannot rule out the possibility that only one isomer reacts with concomitant re-establishment of the equilibrium.

When a dichloromethane solution of **1** is photolysed, **2** and **3** are again produced although the conversion appears to favour **2** over **3** to a greater extent than under the conditions for the spontaneous cluster assembly described above. Again, **1a** and **1b** are consumed at equal rates. Photolytic conditions typically produced **2**/**3** in a ratio (based on ^{11}B NMR integrals) of 5/1 in 16 h compared to 2/1.5 (with unreacted **1** still present) after a month without a source of direct irradiation.

Compound **3** was first reported and crystallographically characterised by Shore and coworkers [5]. We have independently described the synthesis and spectroscopic characterisation of $[\mathbf{3}]^-$, viz. $[HNMe_3][Ru_6(CO)_{17}B]$ [12], and the solution properties correspond well with those reported for $[PPN][Ru_6(CO)_{17}B]$ [5]. After **3** had been separated from the products of the photolysis of **1**, mass spectroscopic data indicated the presence both of **3** ($m/z = 1095$) and a higher nuclearity species with $m/z = 1576$. This parent envelope gave rise to a series of fragmentation peaks consistent with the loss of at least fifteen carbonyl ligands. The mass and isotopic distribution of the P^+ envelope corresponded to a formulation of $Ru_9(CO)_{23}B_2$ (m/z(calc) = 1575). Assuming that the boron atoms are interstitial and that each therefore provides 3 electrons for cluster bonding, such a species would possess 124 valence electrons. This electron count is consistent with a core structure consisting of two face sharing octahedra (viz. $(2 \times 86) - 48$ electrons) (Fig. 1) [13]. Attempts to separate the fraction further by TLC were unsuccessful. Recrystallisation at $-20\,^{\circ}C$ from dichloromethane layered with hexane yielded deep red crystals, a solution (CH_2Cl_2) infrared spectrum of which was rather more simple than that reported for $HRu_6(CO)_{17}B$ in the same solvent [5]. Observed ν(CO) were 2064vs, 2053s and 2036m cm^{-1} compared to published values of 2079s, 2065vs, 2049s and 2028s cm^{-1}. We therefore decided to undertake a structural investigation of the crystals. The space group and cell dimensions determined for the chosen crystal did not match those reported by Shore et al. for $HRu_6(CO)_{17}B$ but the cell size was inconsistent with the formulation $Ru_9(CO)_{23}B_2$. The crystal proved to be a second isomer of **3**, labelled here as **3a**; differences in geometrical parameters between the present structure and that reported by Shore, referred to here as **3b**, are discussed below.

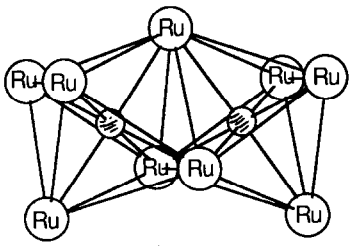

Fig. 1. Proposed core structure of $Ru_9(CO)_{23}B_2$.

Molecular structure of 3a

The molecular structure of **3a** is shown in Fig. 2 and selected bond distances and angles are given in Table 3. The boron atom resides within a distorted octahedral array of ruthenium atoms and is within bonding distance of all six metal atoms; Ru–B distances lie in the range 2.066–2.121 Å. The Ru_6-core exhibits Ru–Ru edge distances in the range 2.824–3.198 Å. Of the seventeen carbonyl ligands, fourteen are terminally bound. Ligands C(6)O(6) and C(11)O(11) are edge bridging and C(17)O(17) is weakly semi-bridging with Ru(6)–C(17) 1.953 and Ru(4)–C(17) 2.882 Å. The hydride ligand, observed in the ^1H NMR spectrum at δ −18.2, was not located directly by X-ray diffraction. Inspection of the Ru_6-core and of the carbonyl ligand orientations in **3a** shows that the carbonyl groups associated with Ru(2) and Ru(6) are bent away from the Ru(2)–Ru(6) vector. This implies that the hydride ligand bridges this edge and the rather long Ru(2)–Ru(6)

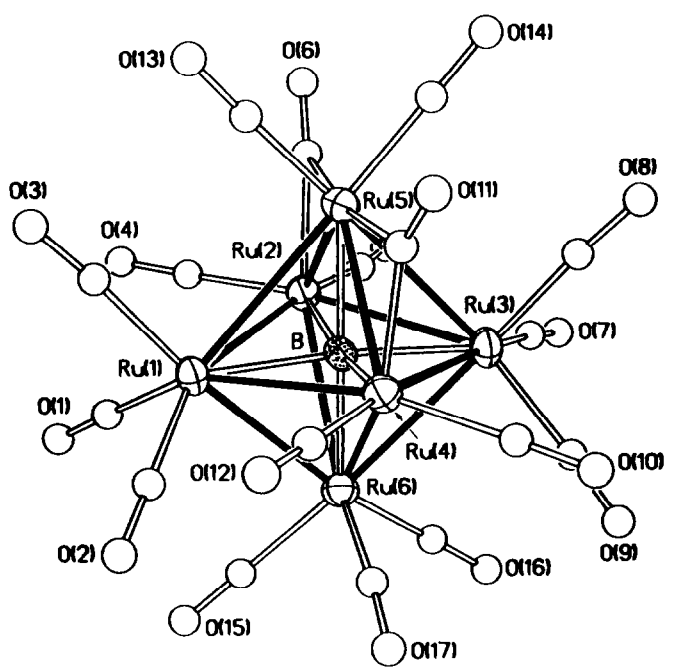

Fig. 2. Molecular structure of **3a** showing atom-labelling scheme. The hydride ligand was not located. The atoms of the CO groups are shown with arbitrary sized spheres for clarity.

Table 3

Selected bond distances (Å) and angles (°) for **3a**

Ru(1)–Ru(2)	2.948(1)	Ru(1)–Ru(4)	2.957(1)
Ru(1)–Ru(5)	3.048(1)	Ru(1)–Ru(6)	2.881(1)
Ru(1)–B	2.077(5)	Ru(2)–Ru(5)	2.840(1)
Ru(2)–Ru(3)	3.002(1)	Ru(2)–B	2.075(6)
Ru(2)–Ru(6)	3.009(1)	Ru(3)–Ru(4)	2.899(1)
Ru(3)–Ru(5)	3.011(1)	Ru(3)–Ru(6)	2.886(1)
Ru(3)–B	2.066(5)	Ru(4)–B	2.114(6)
Ru(4)–Ru(5)	2.824(1)	Ru(5)–B	2.121(6)
Ru(6)–B	2.097(6)	Ru(4)–Ru(6)	3.198(1)
Ru(2)–Ru(1)–Ru(4)	89.8(1)	Ru(4)–Ru(1)–Ru(5)	56.1(1)
Ru(4)–Ru(1)–Ru(6)	66.4(1)	Ru(1)–Ru(2)–Ru(3)	88.1(1)
Ru(3)–Ru(2)–Ru(5)	62.0(1)	Ru(3)–Ru(2)–Ru(6)	57.4(1)
Ru(2)–Ru(3)–Ru(4)	89.9(1)	Ru(4)–Ru(3)–Ru(5)	57.1(1)
Ru(4)–Ru(3)–Ru(6)	67.1(1)	Ru(1)–Ru(4)–Ru(3)	89.9(1)
Ru(3)–Ru(4)–Ru(5)	63.5(1)	Ru(1)–Ru(5)–Ru(3)	86.1(1)
Ru(1)–Ru(5)–Ru(4)	60.3(1)	Ru(3)–Ru(5)–Ru(4)	59.5(1)
Ru(2)–Ru(1)–Ru(5)	56.5(1)	Ru(2)–Ru(1)–Ru(6)	62.1(1)
Ru(5)–Ru(1)–Ru(6)	90.6(1)	Ru(1)–Ru(2)–Ru(5)	63.5(1)
Ru(1)–Ru(2)–Ru(6)	57.8(1)	Ru(5)–Ru(2)–Ru(6)	92.2(1)
Ru(2)–Ru(3)–Ru(5)	56.4(1)	Ru(2)–Ru(3)–Ru(6)	61.4(1)
Ru(5)–Ru(3)–Ru(6)	91.3(1)	Ru(1)–Ru(4)–Ru(5)	63.6(1)
Ru(1)–Ru(5)–Ru(2)	60.0(1)	Ru(2)–Ru(5)–Ru(3)	61.7(1)
Ru(2)–Ru(5)–Ru(4)	94.8(1)	Ru(1)–Ru(6)–Ru(3)	91.7(1)
Ru(1)–Ru(6)–Ru(2)	60.0(1)	Ru(2)–Ru(6)–Ru(3)	61.2(1)

distance of 3.009(1) Å is consistent with this suggestion. Although several other edges are also somewhat elongated (see Table 3), none is suitable for the location of a bridging hydrogen atom; the semi-bridging carbonyl ligand blocks Ru(4)–Ru(6) while edges Ru(1)–Ru(2), Ru(1)–Ru(5), Ru(1)–Ru(4) and Ru(2)–Ru(3) are not associated with suitably directionalised carbonyl ligands. A projection of the structure of **3a** along the vector Ru(1) · · · Ru(3) is shown in Fig. 3a; the hydride ligand has been positioned equidistant (1.8 Å) from Ru(2) and Ru(6). The cluster has a distinct equatorial plane containing Ru(2,4,5,6), the hydride and three bridging (or semi-bridging) carbonyl ligands in which the maximum metal atom deviation from the plane is less than 0.01 Å and C(11) deviates by 0.21 Å. Each ruthenium atom in the plane carries two terminal carbonyl ligands while each apical ruthenium atom bears three carbonyl ligands.

The geometry described here for **3a** exhibits some significant differences from that reported for **3b** by Shore and coworkers [5] and the major distinctive features may be appreciated by comparing Fig. 3a with Fig. 3b. In the latter diagram, a projection of **3b** [14*] is given along the corresponding axis to Ru(1) · · · Ru(3) for **3a**. Thus Figs. 3a and 3b are directly comparable. Two features are particularly significant: (i) the apical $Ru(CO)_3$ groups in **3b** are mutually staggered as opposed to being close to eclipsed in **3a**, and (ii) there is one bridging carbonyl ligand [5] and one/two semi-bridging ligand/s (Ru–C = 1.93(2) and 2.59 Å [15*]; Ru–C

* Reference number with asterisk indicates a note in the list of references.

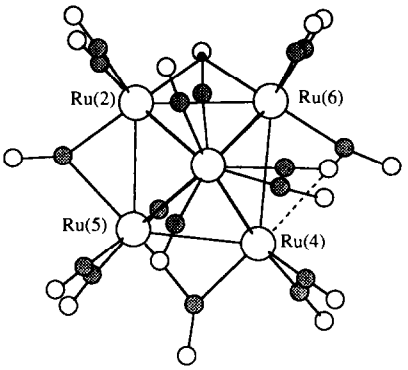

3 a

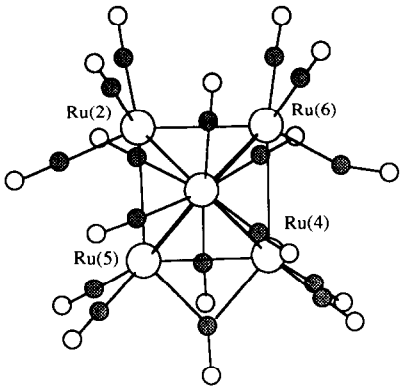

3 b

Fig. 3. Comparative views of $HRu_6(CO)_{17}B$ projected along the axis Ru(1)···Ru(3): **3a** is the isomer reported here and **3b** is that reported by Shore et al. [5].

1.93(2) and 2.92 Å [15*]) in **3b** compared to two fully bridging and one semi-bridging ligand in **3a**. This latter observation may, on its own, seem to be trivial but is in fact important in that such a difference has a direct influence on the arrangement of the carbonyl ligands on the fourth edge of the equatorial plane. Comparison of Figs. 3a and 3b suggests that perhaps Ru(2)–Ru(6) in **3a** is more suited towards accommodating a hydride ligand than is the corresponding edge in **3b**. The differences in structure observed between **3a** and **3b** are too great for the two species to be considered as polymorphs and they are more reasonably considered as different isomeric forms of $HRu_6(CO)_{17}B$. Similar isomerism is not without precedent in transition metal carbonyl cluster chemistry. A pair of isomers that is relevant to the present discussion is observed for $Ru_5(CO)_{15}S$. The square pyramidal Ru_5S-cluster core is common to both isomers, but the carbonyl arrangement in each is different [16].

The solution ^{11}B and ^1H NMR spectroscopic properties of dissolved crystals [17*] of **3a** were virtually identical to those reported by Shore for **3b** [5] and it was not possible to deduce anything meaningful about the presence of one or more isomers in solution. A solution infrared spectrum recorded for **3a** [17*] was, as stated earlier, rather more simple than that reported for **3b** [5]. However, no absorptions due to bridging carbonyl ligands were observed for either **3a** or **3b**. Insufficient crystalline material was available to permit the making of a KBr disc for an infrared spectrum to be obtained for the solid state. The differences in solution infrared spectra may be due to the presence of one of two isomeric forms of $HRu_6(CO)_{17}B$. One very significant difference between our work and that of Shore and coworkers is the method of synthesis of compound **3**. The previously reported route is a thermolytic one involving the reaction of $BH_3 \cdot THF$ with $Ru_3(CO)_{12}$ in toluene at 75 °C for 5 h [5]. The photolytic method described here may well yield a kinetic rather than thermodynamic product. However, one piece of evidence which mitigates against this suggestion is that we have also formed **3** by heating a toluene solution of **1** for 5 h at 85°C and the infrared spectrum of **3**

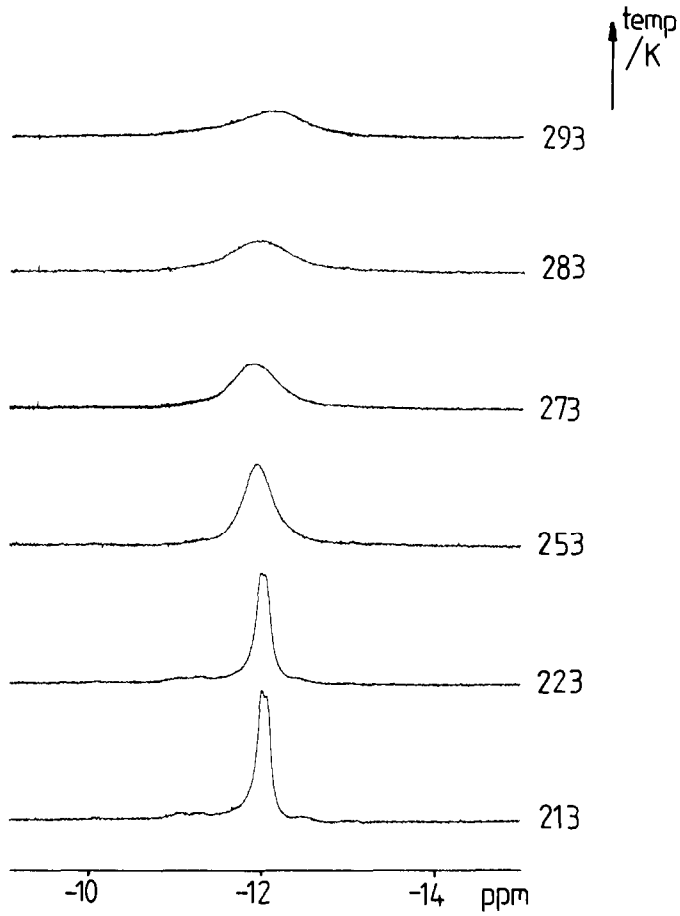

Fig. 4. Variable temperature 250 MHz ^{1}H NMR spectrum (highfield region only) of a CD_2Cl_2 solution of [PPN][$Ru_3(CO)_9BH_4$].

derived by this method is identical to that obtained by the photolytic procedure. We therefore propose that **3a** was fortuitously obtained here in preference to **3b** as a result of specific conditions of crystallisation.

Formation of $[HRu_3Fe(CO)_{12}BH]^-$ and $HRu_3Fe(CO)_{12}BH_2$

The inherent reactivity of **1** makes this compound an ideal reagent for the synthesis of heterometallic clusters. The pathway which would allow cluster expansion to occur may be likened to that observed in the reaction of $[Fe_3(CO)_9BH_4]^-$ with $Fe_2(CO)_9$ in toluene at room temperature. This reaction quantitatively yields the butterfly cluster anion $[HFe_4(CO)_{12}BH]^-$ [6,7]. We have prepared the conjugate base of **1** in order to investigate the suitability of the anion as a precursor to higher nuclearity clusters. [PPN][**1**] is readily made by deprotonation of **1** using sodium carbonate in the presence of the $[PPN]^+$ cation. The ^{11}B NMR spectral resonances at δ + 2.8 (**1a**) and +21.0 (**1b**) are replaced by a single signal for $[\mathbf{1}]^-$ at δ + 22.5. The variable temperature ^{1}H NMR spectrum of $[\mathbf{1}]^-$ is shown in Fig. 4. At 293 K, there is a single broad resonance at δ − 12.1 corresponding to the

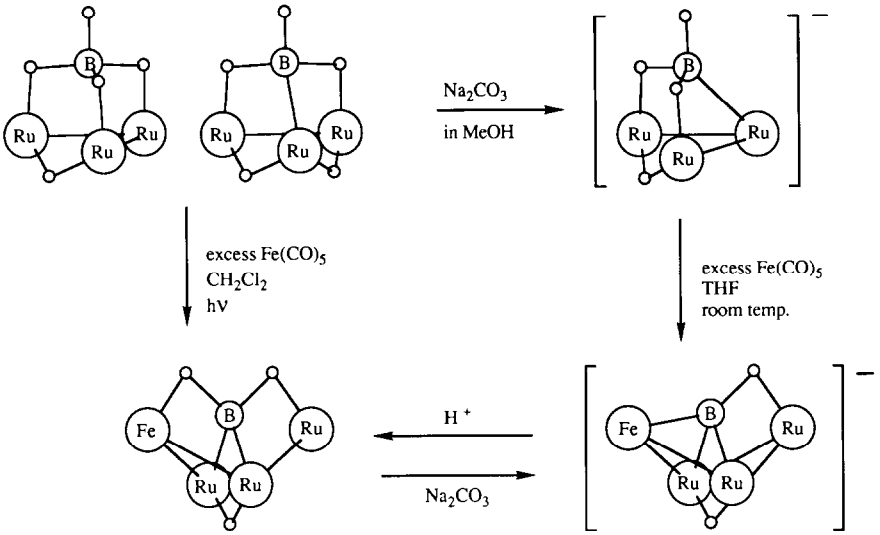

Fig. 5. Proposed structure of $[Ru_3(CO)_9BH_4]^-$ and the reaction sequence leading to the formation of $HRu_3Fe(CO)_{12}BH_2$ (**4**) and its conjugate base. Proposed structures of **4** and $[\mathbf{4}]^-$.

three *endo*-protons. At lower temperatures, the only significant change is the sharpening of this signal; this is attributed to thermal $^{11}B-^1H$ spin decoupling. Although neutral **1** exhibits two isomers over the temperature range shown in Fig. 4, anion $[\mathbf{1}]^-$ exhibits only one form in which the *endo*-hydrogen atoms are either in equivalent Ru–H–B bridging sites or are fluxional between Ru–H–Ru and Ru–H–B sites. For $[Fe_3(CO)_9BH_4]^-$, (viz. the iron analogue of $[\mathbf{1}]^-$), a parallel situation is observed in the ^1H NMR spectrum. In this case, Mössbauer spectroscopy has indicated that the static structure possesses two different iron sites and the anion was proposed as having one Fe–H–Fe and two Fe–H–B hydrogen atoms. We propose that $[\mathbf{1}]^-$ possesses a similar structure to that of its iron analogue (Fig. 5). The ^{11}B NMR chemical shift for $[\mathbf{1}]^-$ is wholly consistent with this suggestion since the observed value of $\delta + 22.5$ implies a similar environment [18] for the boron atom as that present in **1b**. A structure in which there were 3 Ru–H–B bridges would be expected to show a signal in the ^{11}B NMR spectrum at $\delta \approx +3$ (i.e. corresponding to the environment in **1a**).

Rather surprisingly, we have found that, under similar conditions to those used for the successful synthesis of $[HFe_4(CO)_{12}BH]^-$ from $[Fe_3(CO)_9BH_4]^-$, the conjugate base of **1** does not react very readily with $Fe_2(CO)_9$. However, it does react with an excess of $Fe(CO)_5$ to give $[HRu_3Fe(CO)_{12}BH]^-$, but only in yields of $< 10\%$. $[HRu_3Fe(CO)_{12}BH]^-$ can be protonated by using CF_3COOH to give neutral $HRu_3Fe(CO)_{12}BH_2$ (**4**). A more efficient route to the mixed metal cluster is the photolysis of **1** in the presence of excess $Fe(CO)_5$ (Fig. 5). This route yields neutral **4** in $\approx 60\%$ yield. The presence of an excess (typically $\geqslant$ 10-fold) of $Fe(CO)_5$ is essential for optimising the yield of **4**. Photolysis of a dichloromethane solution containing equimolar quantities of **1** and $Fe(CO)_5$ leads to the formation of only a small quantity of **4** with the preferential formation of **2** and **3** being the dominant pathway.

Table 4

Comparative NMR spectroscopic data (in ppm) for $HM_3M'(CO)_{12}BH_2$ and $[HM_3M'(CO)_{12}BH]^-$ (M = M' = Fe or Ru; M = Ru, M' = Fe)

Compound	Solvent	NMR		Reference
		$\delta(^{11}B)$	$\delta(^1H)$	
$HRu_4(CO)_{12}BH_2$	$CDCl_3$ [a]	+109.9	−8.4 (Ru–H–B) −21.18 (Ru–H–Ru)	[3,4]
$HRu_3Fe(CO)_{12}BH_2$	$CDCl_3$	+114	−8.7 (Ru–H–B) −11.2 (Fe–H–B) −20.5 (Ru–H–Ru)	this work
$HFe_4(CO)_{12}BH_2$	C_6D_6	+116	−11.9 (Fe–H–B) −25.4 (Fe–H–Fe)	[19,20]
$[HRu_4(CO)_{12}BH][PPN]$ [b]	$(CD_3)_2CO$	+142.2	−6.7 (Ru–H–B) −20.92 (Ru–H–Ru)	[3,4]
$[HRu_3Fe(CO)_{12}BH][PPN]$	CD_2Cl_2	+143.5	−6.5 (Ru–H–B) −20.5 (Ru–H–Ru)	this work
$[HFe_4(CO)_{12}BH][PPN]$	CD_2Cl_2	+150.0	−8.5 (Fe–H–B) −24.9 (Fe–H–Fe)	[6,20]

[a] Chemical shifts are sensitive to solvent; in $(CD_3OCD_2)_2$ the ^{11}B NMR shift for $HRu_4(CO)_{12}BH_2$ is δ +113.5 ppm [4]. [b] The potassium salt exhibits an ^{11}B NMR resonance at δ +140.9 ppm [4].

Compound **4** is related to **2** by the replacement of one ruthenium by an iron atom. It is also related to the tetraferraborane, $HFe_4(CO)_{12}BH_2$ [19–21] and is isoelectronic with the nitrido-cluster $HRu_3Fe(CO)_{12}N$ [22–24]. The iron atom in **4** may reside in either one of the wingtip or hinge sites of the butterfly framework. Simple consideration of the synthetic origins of **4** (Fig. 5) would suggest that the Fe atom is located in a wingtip site. This proposal is corroborated by the NMR spectroscopic data, and in particular by the ^1H NMR data given in Table 4. The ^1H NMR spectrum of **4** is shown in Fig. 6. The molecular asymmetry implied by the presence of three rather than two highfield signals in the ^1H NMR spectrum is consistent with a wingtip iron atom. Two of the highfield resonances are broad and are assigned to M–H–B bridging protons. One chemical shift of δ − 8.7 compares well with that in the all ruthenium cluster **2**, while the second at δ − 11.2 is close to the value of −11.9 observed for $HFe_4(CO)_{12}BH_2$ [19] (Table 4). The chemical shift of the resonance assigned to the M–H–M hydride (Fig. 6) is also instructive and supports the presence of an $Fe_{wingtip}$ rather than Fe_{hinge} atom. The observed value of δ − 20.5 in **4** is consistent with the presence of an Ru–H–Ru bridge. An Fe–H–Ru bridge would be expected to give rise to a signal between the limits of δ − 21.18 (Ru–H–Ru in $HRu_4(CO)_{12}BH_2$) and δ − 25.4 (Fe–H–Fe in $HFe_4(CO)_{12}BH_2$). The preference for a wingtip iron atom proposed for **4** is consistent with the structure found by Gladfelter et al. for the isoelectronic compound $HRu_3Fe(CO)_{12}N$ [22–24].

The conjugate base of **4** may be obtained directly via the reaction of $[Ru_3(CO)_9BH_4]^-$ with $Fe(CO)_5$ or by treatment of **4** with mild base. Loss of the resonance at δ − 11.2 in the ^1H NMR spectrum and a shift of the signal at δ − 8.7 to −6.5 (see Table 4) is consistent with the removal of the Fe–H–B bridging proton. The preferential loss of the Fe–H–B rather than Ru–H–B or Ru–H–Ru protons is to be expected on energetic grounds. The spectroscopic data for $[\mathbf{4}]^-$

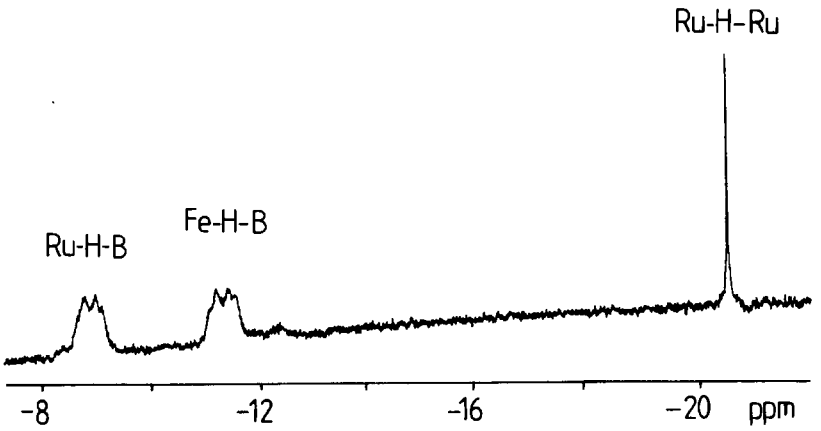

Fig. 6. 400 MHz ^{1}H NMR spectrum of **4** in $CDCl_3$ at 298 K.

suggest that, as in **4**, the iron atom is sited in a wingtip site. This preference contrasts with that for the corresponding nitrido-anion, $[Ru_3Fe(CO)_{12}N]^-$ in which two isomers ($Fe_{wingtip}$ or Fe_{hinge}) are observed [24]. The solid state structure of $[Ru_3Fe(CO)_{12}N]^-$ reveals disordering of the iron atom over both wingtip and hinge sites [23].

In solution and at room temperature, anion $[\mathbf{4}]^-$ exhibits a doublet in its ^{11}B NMR spectrum with J(BH) 90 Hz. This indicates that the *endo*-hydrogen atoms in $[\mathbf{4}]^-$ are static on the NMR timescale and indeed this is confirmed in the ^{1}H NMR spectrum by the observation of two highfield resonances at $\delta - 6.5$ and -20.5 corresponding to the Ru–H–B and Ru–H–Ru protons respectively. The static nature of $[\mathbf{4}]^-$ mimics that of the all ruthenium anion $[\mathbf{2}]^-$ [3] while contrasting with the fluxional nature at 298 K of the iron analogue, $[HFe_4(CO)_{12}BH]^-$ [20]. Both this observation and that of the preferential loss of an Fe–H–B proton when **4** reacts with base may be rationalised on the basis of an increase in the metal–metal bond strengths on descending group 8.

Conclusions

The work described in this paper illustrates the particular reactivity of $Ru_3(CO)_9BH_5$ (**1**) with respect to cluster expansion reactions. The spontaneous transformation of **1** under photolytic conditions to the tetraruthenium cluster **2** and the hexaruthenium boride **3** is of particular interest. In harnessing the reactivity of **1** in order to synthesise the heterometallic cluster **4**, we have noted significant competition between the reaction of **1** with the heterometallic fragment and with itself. The pathway may be swung in favour of **4** only in the presence of a $\geqslant$ 10-fold excess of $Fe(CO)_5$. Work is currently in progress to assess to reactivity of **1** with a range of transition metal carbonyl fragments.

Acknowledgements

Acknowledgements are made to the Donors of the Petroleum Research Fund, administered by the American Chemical Society, for support of this research

(grants #19155-AC3 and #22771-AC3), to the S.E.R.C. for studentships (to S.M.D. and D.M.M.) and to the NSF for a grant (CHE 9007852) towards the purchase of a diffractometer at the University of Delaware. Johnson–Matthey is thanked for generous loans of $RuCl_3$.

References

1 A.K. Chipperfield and C.E. Housecroft, J. Organomet. Chem., 349 (1988) C17.
2 C.R. Eady, B.F.G. Johnson and J. Lewis, J. Chem. Soc., Dalton Trans., (1977) 477.
3 A.K. Chipperfield, C.E. Housecroft and A.L. Rheingold, Organometallics, 9 (1990) 681.
4 F.E. Hong, D.A. McCarthy, J.P. White III, C.E. Cottrell and S.G. Shore, Inorg. Chem., 29 (1990) 2874.
5 F.E. Hong, T.J. Coffy, D.A. McCarthy and S.G. Shore, Inorg. Chem., 28 (1989) 3284.
6 C.E. Housecroft and T.P. Fehlner, Organometallics, 5 (1986) 379.
7 C.E. Housecroft, M.L. Buhl, G.J. Long and T.P. Fehlner, J. Am. Chem. Soc., 109 (1987) 3323.
8 J.W. Kolis, E.M. Holt, J.A. Hriljac and D.F. Shriver, Organometallics, 3 (1984) 496.
9 J.A. Hriljac, P.N. Swepston and D.F. Shriver, Organometallics, 4 (1985) 158.
10 J.A. Hriljac, S. Harris and D.F. Shriver, Inorg. Chem., 27 (1988) 816.
11 C.K. Schauer and D.F. Shriver, Angew. Chem., Int. Ed. Engl., 26 (1987) 255.
12 A.K. Chipperfield, C.E. Housecroft and P.R. Raithby, Organometallics, 9 (1990) 479.
13 D.M.P. Mingos, J. Chem. Soc., Chem. Commun., (1983) 706.
14 The diagram has been generated by using crystallographic coordinates from the supplementary data for **3b** [5].
15 The semi-bonding Ru · · · C distances have been calculated by us using the crystallographic coordinates for **3b**.
16 R.D. Adams, J.E. Babin and M. Tasi, Organometallics, 7 (1988) 503.
17 NMR and IR spectroscopic data were recorded using crystals from the same batch as the one chosen for the X-ray diffraction study.
18 N.P. Rath and T.P. Fehlner, J. Am. Chem. Soc., 110 (1988) 5345.
19 K.S. Wong, W.R. Scheidt and T.P. Fehlner, J. Am. Chem. Soc., 104 (1982) 1111.
20 C.E. Housecroft, M.L. Buhl, G.J. Long and T.P. Fehlner, J. Am. Chem. Soc., 109 (1987) 3323.
21 T.P. Fehlner, C.E. Housecroft, W.R. Scheidt and K.S. Wong, Organometallics, 2 (1983) 825.
22 D.E. Fjare and W.L. Gladfelter, J. Am. Chem. Soc., 103 (1981) 1572.
23 D.E. Fjare and W.L. Gladfelter, J. Am. Chem. Soc., 106 (1984) 4799.
24 M.L. Blohm, D.E. Fjare and W.L. Gladfelter, J. Am. Chem. Soc., 108 (1986) 2301.